

Efficient algorithms for surface density of states in topological photonic and acoustic systems

Yi-Xin Sha,^{1,*} Ming-Yao Xia,² Ling Lu,³ and Yi Yang^{1,†}

¹*Department of Physics and HK Institute of Quantum Science and Technology,
The University of Hong Kong, Hong Kong 999077, China*

²*State Key Laboratory of Advanced Optical Communication Systems and Networks,
School of Electronics, Peking University, Beijing 100871, China*

³*Beijing National Laboratory for Condensed Matter Physics and Institute of Physics,
Chinese Academy of Sciences, Beijing 100190, China*

Robust surface states are a defining feature of topological photonic and acoustic systems. Although the supercell technique is commonly used for studying their surface effects, it falls short in sorting the states at two boundaries, differentiating surface states from bulk states, and demanding large computational resources. To overcome the limitations, we employ surface Green's functions combined with two efficient algorithms to obtain the ideal surface states for a semi-infinite system. They are further extended to more complex scenarios, such as coated structures, heterostructures, and sandwiched structures. Photonic Chern insulators, valley photonic crystals, and acoustic topological insulators are taken as examples for demonstration and verification. The surface spectra obtained from our approach can be directly used for comparison with experimental observables. Our approach enriches the efficient computational tools for topological photonics and acoustics.

INTRODUCTION

Topological photonic and acoustic crystals have emerged as versatile platforms for exploring topological physics, garnering considerable interest these years [1–6]. One of their remarkable features is that their surface states are robust against defects and disorders, which brings potential in realizing useful devices like waveguides, antennas, splitters, and lasers [7–14]. To study the surface effects, calculating the band structure of a supercell (finite-sized slab) has always been the method of choice, but it has several drawbacks. One problem is that it is hard to distinguish the surface states on both sides of the slab unless the eigenfunctions are calculated and examined [15]. Another issue is that the slab thickness should be large enough to avoid the spurious coupling between the surface states at the two boundaries, leading to substantial consumption of computational resources [16]. Most importantly, the surface bands are mixed with the bulk bands, and the results cannot be directly compared with the surface state spectrum measured from the near field scanning experiments [17].

In electronic systems, an effective solution to the above issues is to calculate the surface Green's function for a semi-infinite structure. From this, one can obtain the surface state spectrum at a single well-defined boundary. Numerous algorithms [18] have been proposed to expedite the computation process, primarily falling into two categories. One is the iterative technique, such as the cyclic reduction method (CRM) [19–21], which relies on repeatedly inverting a coupling matrix for a unit cell. The other is the semi-analytical technique, such as the transfer matrix method (TMM) [22–26], which is based on the eigenanalysis of a transfer matrix for a pair of unit cells. These methods deal only with one or two unit cells rather than a large supercell, which greatly reduces memory consumption. Currently, they have been widely used to investigate surface properties of electronic materials [15–17, 27–31] and even developed as a powerful tool for exploring novel topological materials [32].

As for photonic and acoustic systems, similar schemes have also been applied to the surface problem. For example, a CRM in a finite element representation of Hamiltonian is put forward to calculate the surface states of photonic and acoustic topological semimetals [33], but the formulation is limited to the case of a bare semi-infinite structure. A TMM based on plane wave basis set is presented to simulate the wave propagation in more complex cases such as sandwiched photonic crystals [34, 35], but such non-localized basis functions are hard to describe the optical fields in metallic materials and sound waves in rigid bodies.

In order to address the above limitations, in this work, we implement the CRM and TMM using finite element discretization in photonic and acoustic systems and provide the computational paradigms across a variety of scenarios, such as a bare semi-infinite crystal, a semi-infinite crystal with a surface defect, two semi-infinite crystals interfaced with each other, and two semi-infinite crystals with an interface defect. We demonstrate the utility of our approach by calculating the surface state spectra of photonic Chern insulators, valley photonic crystals, and acoustic topological insulators and compare the differences in the computational efficiency and accuracy between the two methods.

COMPUTATIONAL FRAMEWORK

The Green's functions in photonic [Eq. (1a)] and acoustic [Eq. (1b)] systems can be defined as the solutions of the wave equations for a point source:

$$\underbrace{[\nabla \times \boldsymbol{\mu}^{-1}(\mathbf{r}) \cdot \nabla \times - \omega^2 \boldsymbol{\varepsilon}(\mathbf{r})]}_{\mathbf{Z}(\mathbf{r};\omega)} \mathbf{G}(\mathbf{r}, \mathbf{r}'; \omega) = \mathbf{I} \delta(\mathbf{r} - \mathbf{r}'), \quad (1a)$$

$$\underbrace{[\nabla \cdot \rho^{-1}(\mathbf{r}) \nabla + \omega^2 K^{-1}(\mathbf{r})]}_{\mathbf{Z}(\mathbf{r};\omega)} G(\mathbf{r}, \mathbf{r}'; \omega) = \delta(\mathbf{r} - \mathbf{r}'), \quad (1b)$$

where $\boldsymbol{\mu}(\mathbf{r})$, $\boldsymbol{\varepsilon}(\mathbf{r})$, $\rho(\mathbf{r})$ and $K(\mathbf{r})$ are the permeability, permittivity, mass density and bulk modulus at the location \mathbf{r} , respec-

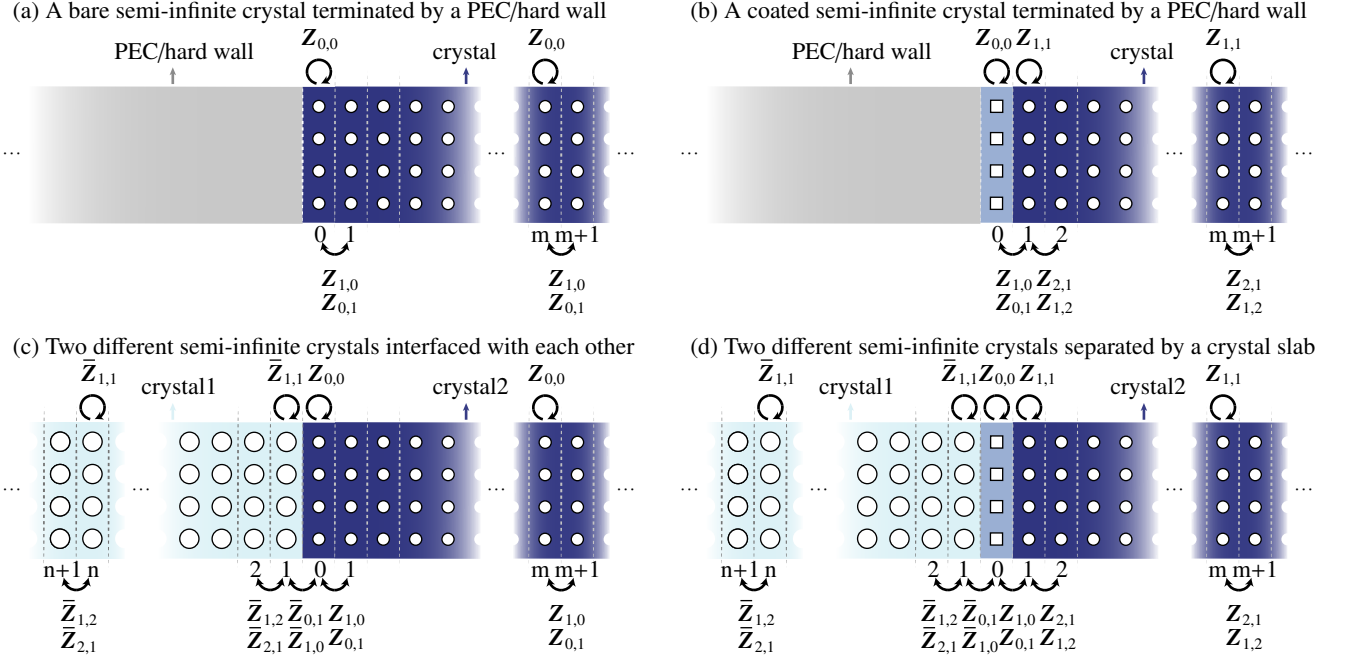


FIG. 1. **Various photonic or acoustic crystal structures which support topological surface states.** The structure is divided into layers along the direction perpendicular to the surface indicated by an index m . $Z_{m,m}$ is the intra-coupling matrix within a single layer, $Z_{m,m+1}$ and $Z_{m+1,m}$ are the inter-coupling matrices between two nearest-neighbor layers. \bar{Z} represents the coupling matrix in the opposite direction. (a) A bare semi-infinite crystal. (b) A semi-infinite coated crystal. (c) Two different semi-infinite crystals interfaced with each other. (d) Two different semi-infinite crystals separated by another crystal slab.

tively. $\delta(\mathbf{r} - \mathbf{r}')$ is a Dirac's delta source at \mathbf{r}' . For simplicity, we write the above equations as $\mathbf{Z}\mathbf{G} = \mathbf{I}$, where \mathbf{Z} combines the differential operators and material parameters, and \mathbf{G} is the Green's function.

Local density of states (LDOS) describes the spatial distribution of the intensity of a single-particle eigenstate, and can be calculated from the imaginary part of \mathbf{G} by imposing an infinitesimal imaginary frequency η [36–38]:

$$\text{LDOS}(\mathbf{r}; \omega) = \frac{2\omega}{\pi} \text{Im} \left\{ \text{Tr} \left[\lim_{\eta \rightarrow 0^+} \mathbf{G}(\mathbf{r}, \mathbf{r}; \omega + i\eta) \right] \right\}, \quad (2a)$$

$$\text{LDOS}(\mathbf{r}; \omega) = \frac{2\omega}{\pi} \text{Im} \left[\lim_{\eta \rightarrow 0^-} G(\mathbf{r}, \mathbf{r}; \omega + i\eta) \right]. \quad (2b)$$

Here Eq. (2a) and Eq. (2b) are the computation expressions for photonic and acoustic systems, respectively. Tr in Eq.(2a) signifies tracing the Green's tensor, as it is necessary to consider all polarization degrees of freedom in a photonic system.

Because this work mainly focuses on the topological states localized at the system boundaries, we define the surface density of states (SDOS) as the integration of LDOS over the surface layer for the following calculations and analyses. Next, we will provide two efficient algorithms to obtain the SDOS of photonic and acoustic crystals.

Cyclic reduction method. Firstly, let us consider a simple case, a bare semi-infinite photonic crystal, as shown in Fig. 1(a). Since we only care about the wave propagating

along the interface, the periodic boundary condition along the closed direction reduces the system to a one-dimensional chain. By discretizing the system with finite elements [39, 40], we obtain a semi-infinite eigenmatrix

$$\mathbf{Z} = \begin{pmatrix} Z_{0,0} & Z_{0,1} & & & \\ Z_{1,0} & Z_{0,0} & Z_{0,1} & & \\ & Z_{1,0} & Z_{0,0} & Z_{0,1} & \\ & & \ddots & \ddots & \ddots \\ & & & Z_{1,0} & Z_{0,0} & Z_{0,1} \\ & & & & \ddots & \ddots & \ddots \end{pmatrix}. \quad (3)$$

\mathbf{Z} takes a block-cyclic tri-diagonal (Toeplitz) form due to the semi-infinite crystal periodicity, and its subscripts represent the layer numbers. The diagonal block $Z_{m,m}$ represents the intra-coupling within the m -th layer, and the off-diagonal blocks $Z_{m,m+1}$ and $Z_{m+1,m}$ denote the inter-couplings between the neighbouring layers.

To solve for the surface Green's function $G_{0,0}$, we now expand Eq. (1) in a block manner according to Eq. (3), which gives a series of chain equations:

$$-\zeta_0 \mathbf{G}_{m,0} = \alpha_0 \mathbf{G}_{m+1,0} + \beta_0 \mathbf{G}_{m-1,0}, \quad (m \geq 1), \quad (4a)$$

$$-\zeta_0^s \mathbf{G}_{0,0} = \alpha_0 \mathbf{G}_{1,0} - \mathbf{I}, \quad (4b)$$

where

$$\alpha_0 = \mathbf{Z}_{0,1}, \beta_0 = \mathbf{Z}_{1,0}, \zeta_0 = \mathbf{Z}_{0,0}, \quad (5a)$$

$$\zeta_0^s = \mathbf{Z}_{0,0}. \quad (5b)$$

Next, we remove the odd-layer Green's functions repeatedly using Gaussian elimination, and Eq. (4)-Eq. (5) are transformed into the following forms after the i -th iterations:

$$-\zeta_i \mathbf{G}_{2^i m, 0} = \alpha_i \mathbf{G}_{2^i(m+1), 0} + \beta_i \mathbf{G}_{2^i(m-1), 0}, \quad (m \geq 1), \quad (6a)$$

$$-\zeta_i^s \mathbf{G}_{0,0} = \alpha_i \mathbf{G}_{2^i, 0} - \mathbf{I}, \quad (6b)$$

where

$$\alpha_i = \alpha_{i-1} (\zeta_{i-1})^{-1} \alpha_{i-1}, \quad (7a)$$

$$\beta_i = \beta_{i-1} (\zeta_{i-1})^{-1} \beta_{i-1}, \quad (7a)$$

$$\zeta_i = \zeta_{i-1} - \alpha_{i-1} (\zeta_{i-1})^{-1} \beta_{i-1} - \beta_{i-1} (\zeta_{i-1})^{-1} \alpha_{i-1},$$

$$\zeta_i^s = \zeta_{i-1}^s - \alpha_{i-1} (\zeta_{i-1})^{-1} \beta_{i-1}. \quad (7b)$$

Here Eq. (6) and Eq. (7) define an effective eigenmatrix which builds connections between the layers at intervals of 2^i . As the iteration proceeds, the distance between those layers will increase exponentially, and the corresponding inter-couplings (α_i and β_i) will decay exponentially to zero due to the inclusion of a global loss [(i.e. η in Eq. (2))].

Finally, the surface Green's function $\mathbf{G}_{0,0}$ decouples with the bulk one $\mathbf{G}_{2^i, 0}$ in Eq. (6b), and we achieve its approximation

$$\mathbf{G}_{0,0} = \lim_{i \rightarrow \infty} (\zeta_i^s)^{-1}, \quad (8)$$

which in turn allows for the derivation of the SDOS through Eq. (2).

Aside from the bare semi-infinite scenario described above, the CRM can also handle other more complicated situations like (line defects between) heterostructures, as shown in Fig. 1(b)-(d). Their associated pseudo-codes can be found in Algorithm. 2- 4.

Transfer matrix method (TMM). Complementary to the CRM, in the following, we describe the TMM for SDOS, which is of higher accuracy at the cost of reduced computational speed. Similar to the previous subsection, we choose the bare semi-infinite structure shown in Fig 1(a) as the example for elaboration. We can relate the Green's functions of each layer by introducing a transfer matrix \mathbf{T} , which also corresponds to Eq. (4):

$$\begin{pmatrix} \mathbf{G}_{m+1,0} \\ \mathbf{G}_{m,0} \end{pmatrix} = \mathbf{T}^m \begin{pmatrix} \mathbf{G}_{1,0} \\ \mathbf{G}_{0,0} \end{pmatrix}, \quad (m \geq 1), \quad (9a)$$

$$-\mathbf{Z}_{0,0} \mathbf{G}_{0,0} = \mathbf{Z}_{0,1} \mathbf{G}_{1,0} - \mathbf{I}, \quad (9b)$$

with

$$\mathbf{T} = \begin{pmatrix} -\mathbf{Z}_{0,1}^{-1} \mathbf{Z}_{0,0} & -\mathbf{Z}_{0,1}^{-1} \mathbf{Z}_{1,0} \\ \mathbf{I} & \mathbf{0} \end{pmatrix}. \quad (10)$$

Next, we rewrite Eq. (9a) in the following form

$$\begin{pmatrix} \mathbf{G}_{m+1,0} \\ \mathbf{G}_{m,0} \end{pmatrix} = \mathbf{S} \mathbf{\Lambda}^m \left[\mathbf{S}^{-1} \begin{pmatrix} \mathbf{G}_{1,0} \\ \mathbf{G}_{0,0} \end{pmatrix} \right], \quad (11)$$

where $\mathbf{\Lambda}$ is a diagonal matrix and \mathbf{S} is a full matrix consisting of all the eigenvalues and eigenvectors of \mathbf{T} , respectively:

$$\mathbf{T} \mathbf{S} = \mathbf{S} \mathbf{\Lambda}. \quad (12)$$

Upon analyzing Eq. (11), it becomes imperative to eliminate the eigenvalues of $\mathbf{\Lambda}$ with moduli greater than 1 to avoid divergence in the Green's functions ($\mathbf{\Lambda}^m = \infty$). Consequently, the term enclosed within the square brackets must satisfy the following condition:

$$\mathbf{S}^{-1} \begin{pmatrix} \mathbf{G}_{1,0} \\ \mathbf{G}_{0,0} \end{pmatrix} = \begin{pmatrix} \mathbf{C} \\ \mathbf{0} \end{pmatrix}, \quad (13)$$

where \mathbf{C} is a constant matrix, $\mathbf{0}$ is a zero matrix, and their positions correspond to those of eigenvalues with moduli less than 1 and greater than 1 in $\mathbf{\Lambda}$, respectively. Then \mathbf{S} can also be arranged as a partition matrix corresponding to the same eigenvalue distribution in $\mathbf{\Lambda}$:

$$\mathbf{S} = \begin{pmatrix} \mathbf{S}_2 & \mathbf{S}_4 \\ \mathbf{S}_1 & \mathbf{S}_3 \end{pmatrix}. \quad (14)$$

Substituting Eq. (14) into Eq. (13), we have a relationship between the surface Green's function $\mathbf{G}_{0,0}$ and the bulk one $\mathbf{G}_{1,0}$:

$$\begin{pmatrix} \mathbf{G}_{1,0} \\ \mathbf{G}_{0,0} \end{pmatrix} = \mathbf{S} \begin{pmatrix} \mathbf{C} \\ \mathbf{0} \end{pmatrix} = \begin{pmatrix} \mathbf{S}_2 \mathbf{C} \\ \mathbf{S}_1 \mathbf{C} \end{pmatrix} \implies \mathbf{G}_{1,0} = \mathbf{S}_2 \mathbf{S}_1^{-1} \mathbf{G}_{0,0}. \quad (15)$$

Finally, combining Eq. (15) with Eq. (9b), we obtain an explicit expression for the surface Green's function:

$$\mathbf{G}_{0,0} = (\mathbf{Z}_{0,0} + \mathbf{Z}_{0,1} \mathbf{S}_2 \mathbf{S}_1^{-1})^{-1}, \quad (16)$$

and the SDOS for the semi-infinite system can be accordingly derived via Eq. (2).

One potential difficulty may arise when the inverse of the inter-coupling matrix $\mathbf{Z}_{0,1}$ in Eq. (10) does not exist. To overcome the problem, one can decompose the transfer matrix in the following way:

$$\mathbf{T} = \mathbf{T}_1^{-1} \mathbf{T}_2 = \begin{pmatrix} \mathbf{0} & \mathbf{I} \\ -\mathbf{Z}_{0,1} & \mathbf{0} \end{pmatrix}^{-1} \begin{pmatrix} \mathbf{I} & \mathbf{0} \\ \mathbf{Z}_{0,0} & \mathbf{Z}_{1,0} \end{pmatrix}, \quad (17)$$

and transform the standard eigenvalue problem [see Eq. (12)] into a generalized eigenvalue problem to find the eigensolutions of \mathbf{T} [24].

The detailed pseudo-codes of using TMM to handle other complex structures, as shown in Fig 1(b)-(d), are summarized in Algorithm. 6- 8.

NUMERICAL EXAMPLES

To showcase the applicability of the CRM and TMM in different complex scenarios, we select four representative photonic structures (see Fig 2-Fig 5) for verification, which correspond to the four cases illustrated in Fig 1(a)-(d). Moreover, we include another two structures (see Fig 6-Fig 7) to demonstrate that these methods are equally effective for 1. both crystal-crystal and homogeneous-media-crystal interfaces; and 2. both photonic and acoustic systems. For all of these six examples, we assume continuous translational invariance along the z direction with $k_z = 0$, and introduce the same imaginary frequency $\eta = \omega/1000$ into the original Hermitian systems for a proper broadening of SDOS. In the following, we will give the detailed explanations of these examples.

The first example is a two-dimensional (2D) gyromagnetic photonic Chern insulator with a perfect electric conductor (PEC) cladding [Fig. 1(a)], which exhibits topological surface states in the second band gap. Fig. 2(a) presents a schematic of the structure, and the radii of the dielectric pillars are $0.13a$, with the relative permittivity ϵ_r of 13 and permeability μ_r of $\begin{pmatrix} 1 & -0.4i & 0 \\ 0.4i & 1 & 0 \\ 0 & 0 & 1 \end{pmatrix}$. We calculate the surface band structure for a 12-cell crystal slab and the SDOS for a bare semi-infinite crystal, which are displayed in Fig. 2(b) and Fig. 2(c), respectively. It can be clearly seen that the surface states become more pronounced against the bulk states, and only the chiral state on a single surface is retained in the SDOS spectrum.

Our second example is again, a 2D photonic Chern insulator, but with a surface modification and a PEC cladding [Fig. 1(b)], which features topological slow light in the second band gap. Fig. 3(a) is a schematic of the structure, where the radii of the dielectric pillars are $0.15a$, with the relative permeability μ_r of $\begin{pmatrix} 0.83 & -0.42i & 0 \\ 0.42i & 0.83 & 0 \\ 0 & 0 & 1 \end{pmatrix}$. The relative permittivity ϵ_r of the pillars are $\{15, 15, 25\}$ for adjacent columns along the x direction while kept uniform along the y direction. The surface band structure for a 13-cell crystal slab and the SDOS for a semi-infinite coated crystal are calculated and shown in Fig. 3(b) and Fig. 3(c), respectively. It can be observed that only topological states with negative group velocities are present in the SDOS spectrum, and they exhibit minimal group velocities at the Brillouin zone boundary.

The third example is a 2D valley photonic-crystal heterostructure [Fig. 1(c)], which supports valley-dependent surface states in the second band gap [41]. Fig. 4(a) provides a schematic of the structure, which is composed of two types of dielectric pillars with opposite orientations. The pillar has a side length of $0.615a$ and a chamfer length of $0.11a$ at the corner, with the relative permittivity ϵ_r of 13 and permeability μ_r of 1. We calculate the surface band structure for a 24-cell crystal slab and the SDOS for a heterostructure infinitely extending into both bulks, which are displayed in Fig. 4(b)

and Fig. 4(c), respectively. It becomes apparent that a pair of topological states with opposite group velocities are locked in different valleys in the SDOS spectrum.

The fourth example is again, a valley photonic-crystal heterostructure, but with a line defect sandwiched at the interface [Fig. 1(d)], which supports valley-dependent slow light in the first band gap [42]. Fig. 5(a) offers a schematic of the structure, which consists of three types of dielectric crystal slabs. The crystals have a background material relative permittivity ϵ_r of 11.56 and permeability μ_r of 1, with the long and short side of air pillars being $1.3a/\sqrt{3}$ and $0.7a/\sqrt{3}$. The surface band structure for a 25-cell crystal slab and the SDOS for a sandwiched structure extending infinitely in both directions are calculated and shown in Fig. 5(b) and Fig. 5(c), respectively. It can be intuitively observed that only the confined modes of the beared interface exist in the SDOS spectrum, and it shows slow group velocities near the Brillouin zone edge.

The fifth example is a 2D photonic Chern insulator exposed to air, which has topological surface states in the first band gap [43]. Fig. 6(a) is a schematic of the structure, and the radii of the dielectric pillars are $0.2a$, with the relative permittivity ϵ_r of 15.26 and permeability μ_r of $\begin{pmatrix} 0.80 & -0.72i & 0 \\ 0.72i & 0.80 & 0 \\ 0 & 0 & 1 \end{pmatrix}$.

We calculate the surface band structure for a 12-cell crystal slab and the SDOS for a bare semi-infinite crystal interfaced with air, which are shown in Fig. 6(b) and Fig. 6(c), respectively. It is noted that only the state of the air-crystal interface remains in the SDOS spectrum. Moreover, information absent in the surface band calculation can be found in the SDOS spectrum: when the topological surface band enters the light cone, it couples to the radiation continuum (in the $x-y$ plane), resulting in their hybridization and the blurring of the SDOS of the surface band.

The last example is a 2D acoustic topological insulator, which has a pseudospin-dependent topological surface states in the second band gap [44]. Fig. 7(a) is a schematic of the structure, and the radii of the rigid bodies on the two sides are $0.3a$ and $0.45a$. We calculate the surface band structure for a 24-cell crystal slab and the SDOS for a heterostructure extending infinitely on both sides, which are shown in Fig. 7(b) and Fig. 7(c), respectively. It can be seen from the SDOS spectrum that two pseudospin-locked counterpropagating acoustic modes are equally excited at the same interface.

To summarize these examples, we can see that the efficient calculation of SDOS provides three unique advantages that complement surface band calculations. First, in SDOS spectra, bulk states become genuinely continuous while surface states remain discrete, allowing for a clear visualization of the evolution of surface states, and, in particular, their behaviors within the continuum in frequency-momentum space. Second, the topological states of a single well-defined surface can be obtained directly from SDOS, mitigating the need to inspect individual wavefunctions of surface bands to sort out the localization on different surfaces. Third, the efficient calculation of SDOS spectra has an experimental advantage: they

can be directly compared with observables in near-field scanning experiments in both photonics and acoustics.

COMPUTING EFFICIENCY AND ACCURACY

Both the CRM and TMM can effectively obtain the surface Green's function, owing to the block-cyclic tridiagonal form of the matrix \mathbf{Z} in such periodic systems. In the following, we will evaluate and compare the strengths and weaknesses of the CRM and TMM, particularly in terms of computational efficiency and accuracy.

In terms of computational memory, CRM is more advantageous than TMM. The TMM's memory consumption primarily comes from the eigenanalysis of matrix \mathbf{T} , while the CRM's originates from inverting the self-coupling matrix ζ^s . Notably, \mathbf{T} has twice the degrees of freedom as ζ^s [see Eq. (5b) and Eq. (10)], leading to larger memory usage in TMM. As shown in Table I, for the same degrees of freedom, TMM's memory consumption is approximately four times that of CRM.

TABLE I. Comparison of the memory costs for the two methods, both growing with $O(N^2)$

Unit cell unknowns (N)	500	1000	2000	4000
Memory for CRM (Mb)	3.82	15.29	61.16	244.68
Memory for TMM (Mb)	15.23	61.04	244.36	1005.30

In terms of computation time, CRM is again more advantageous. Firstly, similar to the principle of memory consumption, the time consumption of the TMM primarily stems from the eigenanalysis of matrix \mathbf{T} , while that of the CRM mainly comes from the inversion of the coupling matrix ζ^s . As \mathbf{T} has twice the degrees of freedom as ζ^s , the time consumption of the TMM is therefore greater. Secondly, although the time complexities for both the eigenanalysis and inversion of equivalent matrices are $O(N^3)$, the proportionality constant for eigenanalysis is larger, leading to a longer computation time for the TMM. Table II presents the computation time required for both methods, showing that the TMM takes significantly longer than the CRM for the same number of degrees of freedom.

TABLE II. Comparison of the time costs for the two methods, both growing with $O(N^3)$

Unit cell unknowns (N)	500	1000	2000	4000
Time for CRM (s)	0.005	0.02	0.16	1.28
Time for TMM (s)	0.63	5.02	65.83	1323.29

^a MATLAB run using an Intel Core i7-12700 CPU (12 cores, 20 threads).

^b The CRM time is for a single iteration.

In terms of computational accuracy, the TMM provides

higher precision than the CRM. As the TMM directly provides an exact expression for the surface Green's function [see Eq. (16)], its results are more accurate compared to the iterative approach used by the CRM [see Eq. (8)]. However, it is important to note that the introduction of imaginary frequency η may lead to singularities in the system [such as exceptional points (EPs)]. In this case, \mathbf{T} becomes an ill-conditioned matrix, which could result in catastrophic round-off error amplification, especially at the edges of the energy bands. One possible approach is to reconstruct the relationship between Green's functions and LDOS [see Eq. (2)] at EPs [45] so that the aforementioned efficient algorithms can be utilized as usual.

Furthermore, although the TMM consumes more time and memory when calculating surface Green's functions, the intermediate variables (eigenvalues $\mathbf{\Lambda}$ and eigenvectors \mathbf{S}) generated during the solving process can be simultaneously utilized to compute other physical quantities, such as surface bands and wave functions [22]. This is another computational advantage of the TMM.

CONCLUSIONS AND OUTLOOK

In this article, we apply two efficient algorithms to calculate the SDOS in photonic and acoustic crystals and investigate the corresponding topological phenomenon. The CRM focuses on efficient solving by reducing computational complexity using Gaussian elimination, while the TMM relies on direct solving through eigenanalysis of a transfer matrix. We provide numerical examples of various topological photonic and acoustic crystals to demonstrate the utility of these methods. The unique advantage of these methods is that they can directly and efficiently obtain and monitor the evolution of the topological states of a single interface, and can be used for direct comparison with experimental data. In addition to the photonic and acoustic systems addressed here, our approach can be similarly applied to other platforms such as circuits, as long as the eigenmatrices (or Hamiltonians) of the system exhibit a similar cyclic tridiagonal form [see Eq. (3)] for periodic structures.

The algorithms can be further extended and applied to non-Hermitian systems, where the calculation expression for LDOS defined by Green's functions [see Eq. (2)] can remain valid if the left and right eigenmodes satisfy the completeness relation [38]. In this case, the algorithms presented in this paper can still be employed for fast evaluation of SDOS. For instance, the algorithm designed for sandwiched structure [as shown in Fig. 1(d)] can be used to find the bound states in the continuum in a photonic crystal slab [46].

Our method can also be generalized for higher-order topological systems [47]. For example, regarding corner states in 2D systems, one can consider a structure that extends infinitely in the \mathbf{a} and \mathbf{b} directions but is finite in the $\mathbf{a} + \mathbf{b}$ direction, where \mathbf{a} and \mathbf{b} are primitive vectors. By taking a supercell in the $\mathbf{a} + \mathbf{b}$ direction as a new unit cell, we can ap-

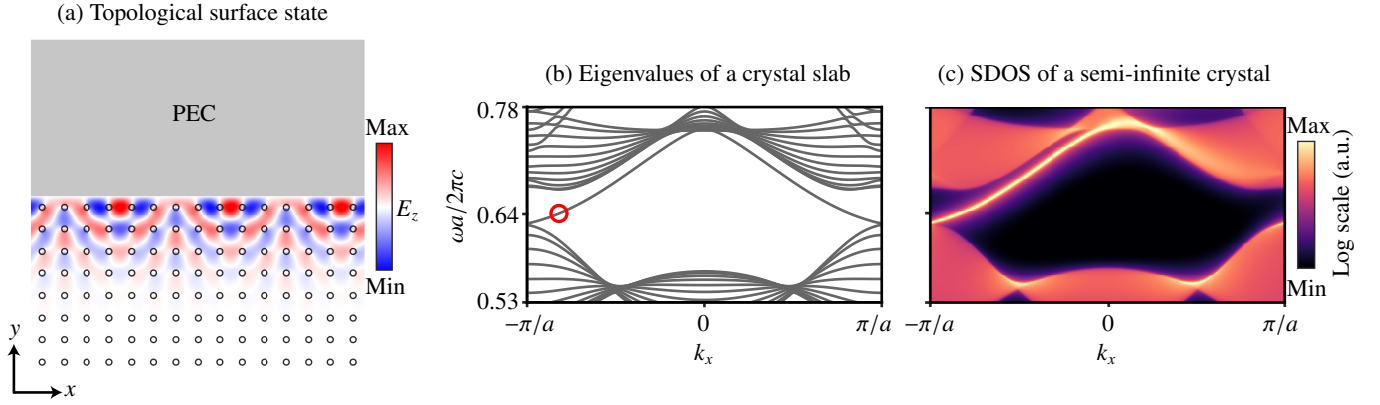


FIG. 2. **Topological surface states of a bare semi-infinite photonic Chern insulator terminated by a PEC.** (a) Mode profile calculated at a normalized frequency of $0.64c/a$, which corresponds to the red circle in (b). (b) Band structure of a 12-cell photonic Chern insulator slab with two PEC boundaries. (c) SDOS spectrum of a semi-infinite photonic Chern insulator with a PEC boundary.

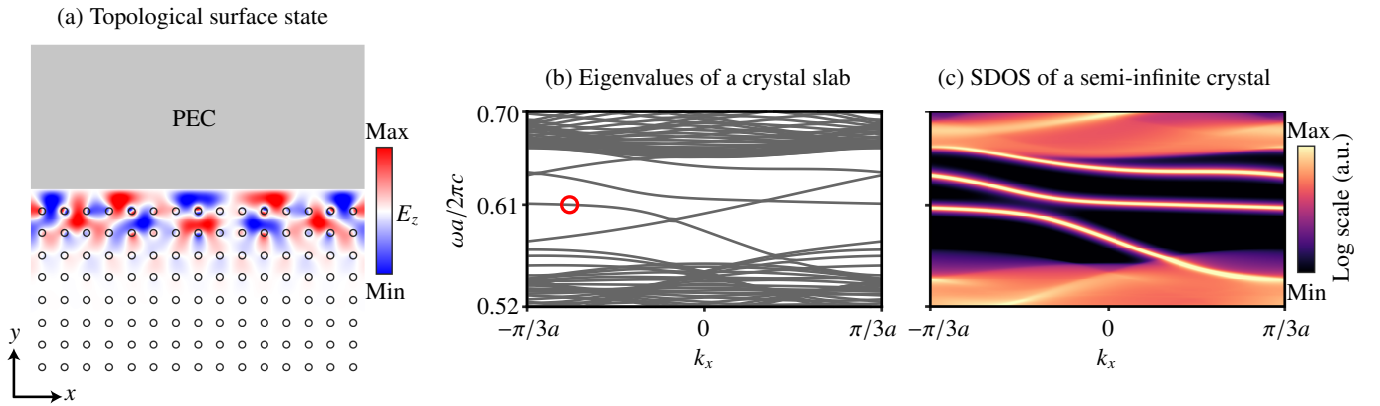


FIG. 3. **Topological surface states of a semi-infinite photonic Chern insulator coated with a crystal slab and terminated by a PEC.** (a) Mode profile calculated at a normalized frequency of $0.61c/a$, which corresponds to the red circle in (b). (b) Band structure of a 13-cell photonic Chern insulator slab with two PEC boundaries. (c) SDOS spectrum of a semi-infinite photonic Chern insulator with a PEC boundary.

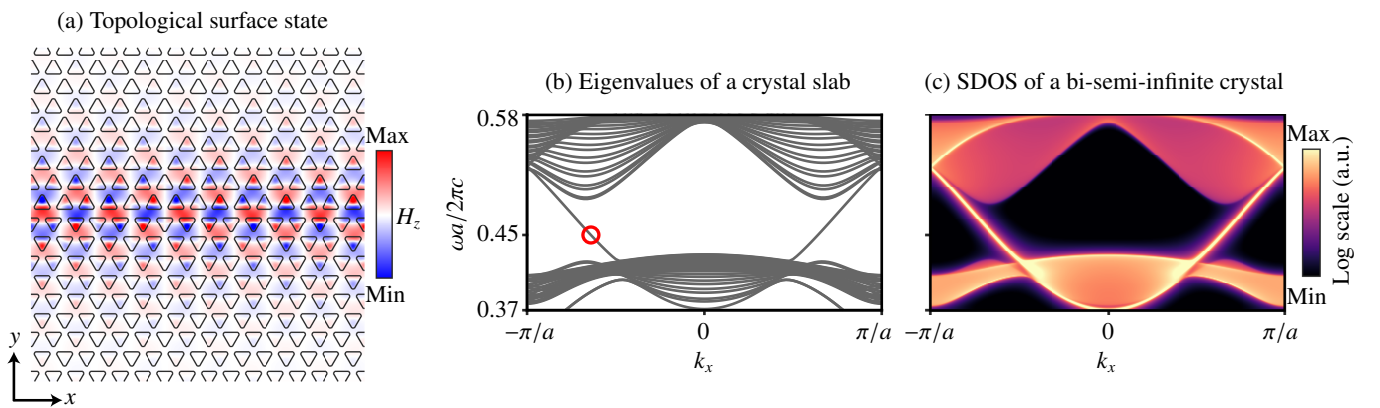


FIG. 4. **Topological surface states of a valley photonic crystal formed by two semi-infinite crystals face to face.** (a) Mode profile calculated at a normalized frequency of $0.45c/a$, which corresponds to the red circle in (b). (b) Band structure of a 24-cell valley photonic crystal slab with two PEC boundaries. (c) SDOS spectrum of a valley photonic crystal extending infinitely on both sides.

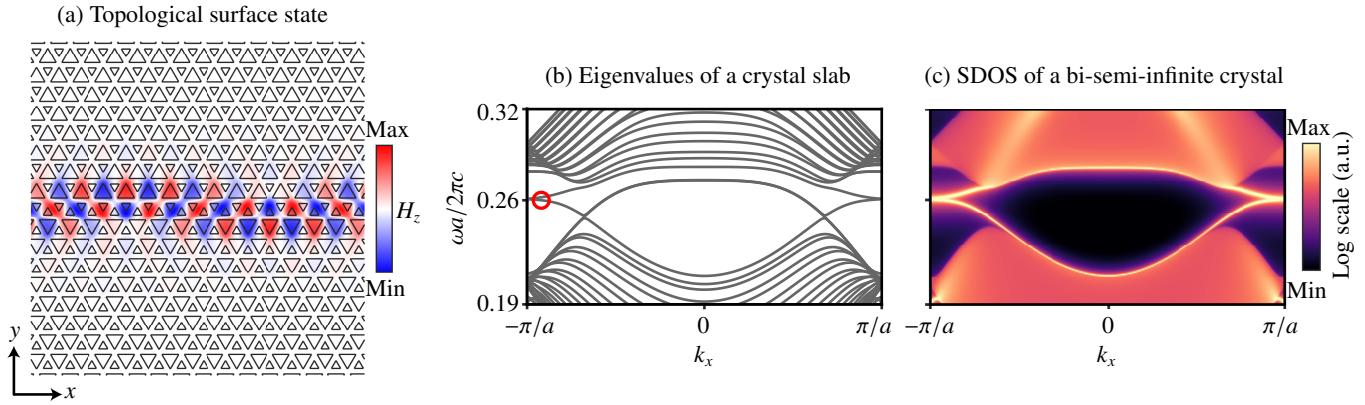


FIG. 5. **Topological surface states of a valley photonic crystal formed by two semi-infinite crystals separated by another crystal slab.** (a) Mode profile calculated at a normalized frequency of $0.26c/a$, which corresponds to the red circle in (b). (b) Band structure of a 25-cell valley photonic crystal slab with two PEC boundaries. (c) SDOS spectrum of a valley photonic crystal extending infinitely on both sides.

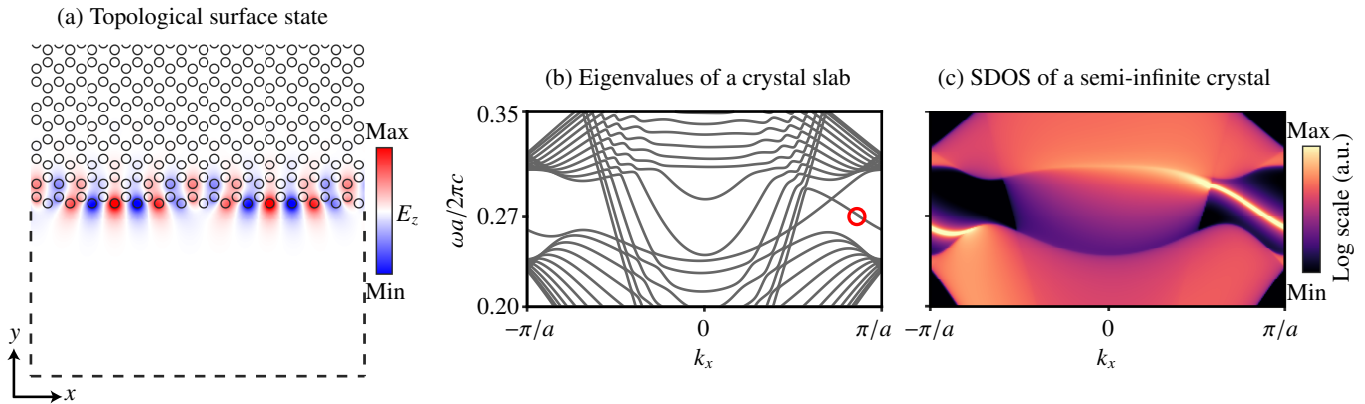


FIG. 6. **Topological surface states of a bare semi-infinite photonic Chern insulator exposed to air.** (a) Mode profile calculated at a normalized frequency of $0.27c/a$, which corresponds to the red circle in (b). (b) Band structure of a 12-cell photonic Chern insulator slab with a PEC and an open boundary. (c) SDOS spectrum of a photonic Chern insulator with an open boundary.

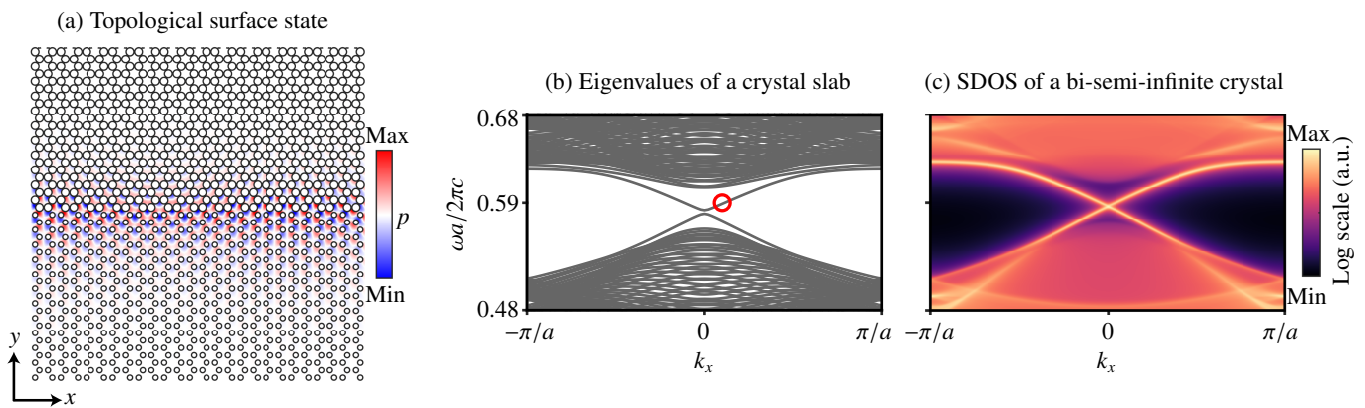


FIG. 7. **Topological surface states of an acoustic topological insulator formed by two semi-infinite crystals face to face.** (a) Mode profile calculated at a normalized frequency of $0.59c/a$, which corresponds to the red circle in (b). (b) Band structure of a 24-cell acoustic topological insulator slab with two hard wall boundaries. (c) SDOS spectrum of an acoustic topological insulator extending infinitely on both sides.

ply the algorithm designed for heterostructures [as shown in Fig. 1(c)] to obtain the corner-density-of-states spectrum.

APPENDIX

Algorithm 1: CRM for a bare semi-infinite crystal

Initialization:

maximum iterations > 0 , error tolerance > 0

$\alpha_0 = \mathbf{Z}_{0,1}$, $\beta_0 = \mathbf{Z}_{1,0}$, $\zeta_0 = \mathbf{Z}_{0,0}$

$\zeta_0^s = \mathbf{Z}_{0,0}$

for $i = 1$ **to** maximum iterations **do**

$\alpha_i = \alpha_{i-1}(\zeta_{i-1})^{-1}\alpha_{i-1}$

$\beta_i = \beta_{i-1}(\zeta_{i-1})^{-1}\beta_{i-1}$

$\zeta_i = \zeta_{i-1} - \alpha_{i-1}(\zeta_{i-1})^{-1}\beta_{i-1} - \beta_{i-1}(\zeta_{i-1})^{-1}\alpha_{i-1}$

$\zeta_i^s = \zeta_{i-1}^s - \alpha_{i-1}(\zeta_{i-1})^{-1}\beta_{i-1}$

if $(\zeta_i^s - \zeta_{i-1}^s)/(\zeta_{i-1}^s) < \text{error tolerance}$ **then**
 | **break**

end

end

$G_{0,0} = (\zeta_i^s)^{-1}$

Algorithm 2: CRM for two semi-infinite crystals interfaced with each other

Initialization:

maximum iterations > 0 , error tolerance > 0

$\alpha_0 = \mathbf{Z}_{0,1}$, $\beta_0 = \mathbf{Z}_{1,0}$, $\zeta_0 = \mathbf{Z}_{0,0}$

$\bar{\alpha}_0 = \bar{\mathbf{Z}}_{1,2}$, $\bar{\beta}_0 = \bar{\mathbf{Z}}_{2,1}$, $\bar{\zeta}_0 = \bar{\mathbf{Z}}_{1,1}$

$\bar{\alpha}_0^s = \bar{\mathbf{Z}}_{0,1}$, $\bar{\beta}_0^s = \bar{\mathbf{Z}}_{1,0}$, $\zeta_0^s = \mathbf{Z}_{0,0}$

for $i = 1$ **to** maximum iterations **do**

$\alpha_i = \alpha_{i-1}(\zeta_{i-1})^{-1}\alpha_{i-1}$

$\beta_i = \beta_{i-1}(\zeta_{i-1})^{-1}\beta_{i-1}$

$\zeta_i = \zeta_{i-1} - \alpha_{i-1}(\zeta_{i-1})^{-1}\beta_{i-1} - \beta_{i-1}(\zeta_{i-1})^{-1}\alpha_{i-1}$

$\bar{\alpha}_i = \bar{\alpha}_{i-1}(\bar{\zeta}_{i-1})^{-1}\bar{\alpha}_{i-1}$

$\bar{\beta}_i = \bar{\beta}_{i-1}(\bar{\zeta}_{i-1})^{-1}\bar{\beta}_{i-1}$

$\bar{\zeta}_i = \bar{\zeta}_{i-1} - \bar{\alpha}_{i-1}(\bar{\zeta}_{i-1})^{-1}\bar{\beta}_{i-1} - \bar{\beta}_{i-1}(\bar{\zeta}_{i-1})^{-1}\bar{\alpha}_{i-1}$

$\bar{\alpha}_i^s = \bar{\alpha}_{i-1}^s(\bar{\zeta}_{i-1})^{-1}\bar{\alpha}_{i-1}$

$\bar{\beta}_i^s = \bar{\beta}_{i-1}^s(\bar{\zeta}_{i-1})^{-1}\bar{\beta}_{i-1}^s$

$\zeta_i^s = \zeta_{i-1}^s - \alpha_{i-1}(\zeta_{i-1})^{-1}\beta_{i-1} - \bar{\alpha}_{i-1}^s(\bar{\zeta}_{i-1})^{-1}\bar{\beta}_{i-1}^s$

if $(\zeta_i^s - \zeta_{i-1}^s)/(\zeta_{i-1}^s) < \text{error tolerance}$ **then**
 | **break**

end

end

$G_{0,0} = (\zeta_i^s)^{-1}$

Algorithm 3: CRM for a semi-infinite coated crystal

Initialization:

maximum iterations > 0 , error tolerance > 0

$\alpha_0 = \mathbf{Z}_{1,2}$, $\beta_0 = \mathbf{Z}_{2,1}$, $\zeta_0 = \mathbf{Z}_{1,1}$

$\alpha_0^s = \mathbf{Z}_{0,1}$, $\beta_0^s = \mathbf{Z}_{1,0}$, $\zeta_0^s = \mathbf{Z}_{0,0}$

for $i = 1$ **to** maximum iterations **do**

$\alpha_i = \alpha_{i-1}(\zeta_{i-1})^{-1}\alpha_{i-1}$

$\beta_i = \beta_{i-1}(\zeta_{i-1})^{-1}\beta_{i-1}$

$\zeta_i = \zeta_{i-1} - \alpha_{i-1}(\zeta_{i-1})^{-1}\beta_{i-1} - \beta_{i-1}(\zeta_{i-1})^{-1}\alpha_{i-1}$

$\alpha_i^s = \alpha_{i-1}^s(\zeta_{i-1})^{-1}\alpha_{i-1}$

$\beta_i^s = \beta_{i-1}^s(\zeta_{i-1})^{-1}\beta_{i-1}^s$

$\zeta_i^s = \zeta_{i-1}^s - \alpha_{i-1}^s(\zeta_{i-1})^{-1}\beta_{i-1}^s$

if $(\zeta_i^s - \zeta_{i-1}^s)/(\zeta_{i-1}^s) < \text{error tolerance}$ **then**
 | **break**

end

end

$G_{0,0} = (\zeta_i^s)^{-1}$

Algorithm 4: CRM for two semi-infinite crystals separated by another crystal slab

Initialization:

maximum iterations > 0 , error tolerance > 0

$\alpha_0 = \mathbf{Z}_{1,2}$, $\beta_0 = \mathbf{Z}_{2,1}$, $\zeta_0 = \mathbf{Z}_{1,1}$

$\bar{\alpha}_0 = \bar{\mathbf{Z}}_{1,2}$, $\bar{\beta}_0 = \bar{\mathbf{Z}}_{2,1}$, $\bar{\zeta}_0 = \bar{\mathbf{Z}}_{1,1}$

$\alpha_0^s = \mathbf{Z}_{0,1}$, $\beta_0^s = \mathbf{Z}_{1,0}$, $\bar{\alpha}_0^s = \bar{\mathbf{Z}}_{0,1}$, $\bar{\beta}_0^s =$

$\bar{\mathbf{Z}}_{1,0}$, $\zeta_0^s = \mathbf{Z}_{0,0}$

for $i = 1$ **to** maximum iterations **do**

$\alpha_i = \alpha_{i-1}(\zeta_{i-1})^{-1}\alpha_{i-1}$

$\beta_i = \beta_{i-1}(\zeta_{i-1})^{-1}\beta_{i-1}$

$\zeta_i = \zeta_{i-1} - \alpha_{i-1}(\zeta_{i-1})^{-1}\beta_{i-1} - \beta_{i-1}(\zeta_{i-1})^{-1}\alpha_{i-1}$

$\bar{\alpha}_i = \bar{\alpha}_{i-1}(\bar{\zeta}_{i-1})^{-1}\bar{\alpha}_{i-1}$

$\bar{\beta}_i = \bar{\beta}_{i-1}(\bar{\zeta}_{i-1})^{-1}\bar{\beta}_{i-1}$

$\bar{\zeta}_i = \bar{\zeta}_{i-1} - \bar{\alpha}_{i-1}(\bar{\zeta}_{i-1})^{-1}\bar{\beta}_{i-1} - \bar{\beta}_{i-1}(\bar{\zeta}_{i-1})^{-1}\bar{\alpha}_{i-1}$

$\alpha_i^s = \alpha_{i-1}^s(\zeta_{i-1})^{-1}\alpha_{i-1}$

$\beta_i^s = \beta_{i-1}^s(\zeta_{i-1})^{-1}\beta_{i-1}^s$

$\bar{\alpha}_i^s = \bar{\alpha}_{i-1}^s(\bar{\zeta}_{i-1})^{-1}\bar{\alpha}_{i-1}$

$\bar{\beta}_i^s = \bar{\beta}_{i-1}^s(\bar{\zeta}_{i-1})^{-1}\bar{\beta}_{i-1}^s$

$\zeta_i^s = \zeta_{i-1}^s - \alpha_{i-1}^s(\zeta_{i-1})^{-1}\beta_{i-1}^s - \bar{\alpha}_{i-1}^s(\bar{\zeta}_{i-1})^{-1}\bar{\beta}_{i-1}^s$

if $(\zeta_i^s - \zeta_{i-1}^s)/(\zeta_{i-1}^s) < \text{error tolerance}$ **then**
 | **break**

end

end

$G_{0,0} = (\zeta_i^s)^{-1}$

Algorithm 5: TMM for a bare semi-infinite crystal

Initialization:

$$T_1 = \begin{pmatrix} \mathbf{0} & I \\ -Z_{0,1} & \mathbf{0} \end{pmatrix}, T_2 = \begin{pmatrix} I & \mathbf{0} \\ Z_{0,0} & Z_{1,0} \end{pmatrix}$$

Eigenanalysis $T_2S = T_1SA$

\ \ sort all the eigenvalues λ and the corresponding eigenvectors s in Λ and S

```

for  $i = 1$  to length( $T_1$ ) do
  for  $j =$  length( $T_1$ ) to  $i + 1$  do
    if  $|\lambda(j)| < |\lambda(j - 1)|$  then
      swap  $\lambda(j)$  with  $\lambda(j - 1)$ 
      swap  $s(j)$  with  $s(j - 1)$ 
    end
  end
end

```

\ \ obtain partitioned $S = \begin{pmatrix} S_1 & S_3 \\ S_2 & S_4 \end{pmatrix}$

$$G_{0,0} = (Z_{0,0} + Z_{0,1}S_2S_1^{-1})^{-1}$$

Algorithm 6: TMM for two semi-infinite crystals interfaced with each other

Initialization:

$$T_1 = \begin{pmatrix} \mathbf{0} & I \\ -Z_{0,1} & \mathbf{0} \end{pmatrix}, T_2 = \begin{pmatrix} I & \mathbf{0} \\ Z_{0,0} & Z_{1,0} \end{pmatrix},$$

$$\bar{T}_1 = \begin{pmatrix} \mathbf{0} & I \\ -\bar{Z}_{1,2} & \mathbf{0} \end{pmatrix}, \bar{T}_2 = \begin{pmatrix} I & \mathbf{0} \\ \bar{Z}_{1,1} & \bar{Z}_{2,1} \end{pmatrix}$$

Eigenanalysis $T_2S = T_1SA$

\ \ sort all the eigenvalues λ and the corresponding eigenvectors s in Λ and S

```

for  $i = 1$  to length( $T_1$ ) do
  for  $j =$  length( $T_1$ ) to  $i + 1$  do
    if  $|\lambda(j)| < |\lambda(j - 1)|$  then
      swap  $\lambda(j)$  with  $\lambda(j - 1)$ 
      swap  $s(j)$  with  $s(j - 1)$ 
    end
  end
end

```

\ \ obtain partitioned $S = \begin{pmatrix} S_1 & S_3 \\ S_2 & S_4 \end{pmatrix}$

Eigenanalysis $\bar{T}_2\bar{S} = \bar{T}_1\bar{S}\bar{A}$

\ \ sort all the eigenvalues $\bar{\lambda}$ and the corresponding eigenvectors \bar{s} in $\bar{\Lambda}$ and \bar{S}

```

for  $i = 1$  to length( $\bar{T}_1$ ) do
  for  $j =$  length( $\bar{T}_1$ ) to  $i + 1$  do
    if  $|\bar{\lambda}(j)| < |\bar{\lambda}(j - 1)|$  then
      swap  $\bar{\lambda}(j)$  with  $\bar{\lambda}(j - 1)$ 
      swap  $\bar{s}(j)$  with  $\bar{s}(j - 1)$ 
    end
  end
end

```

\ \ obtain partitioned $\bar{S} = \begin{pmatrix} \bar{S}_2 & \bar{S}_4 \\ \bar{S}_1 & \bar{S}_3 \end{pmatrix}$

$$G_{0,0} = [Z_{0,0} + Z_{0,1}S_2S_1^{-1} + \bar{Z}_{0,1}(\bar{Z}_{1,1} + \bar{Z}_{1,2}\bar{S}_2\bar{S}_1^{-1})^{-1}\bar{Z}_{1,0}]^{-1}$$

Algorithm 7: TMM for a semi-infinite coated crystal

Initialization:

$$T_1 = \begin{pmatrix} \mathbf{0} & I \\ -Z_{1,2} & \mathbf{0} \end{pmatrix}, T_2 = \begin{pmatrix} I & \mathbf{0} \\ Z_{1,1} & Z_{2,1} \end{pmatrix}$$

Eigenanalysis $T_2S = T_1SA$

\ \ sort all the eigenvalues λ and the corresponding eigenvectors s in Λ and S

```

for  $i = 1$  to length( $T_1$ ) do
  for  $j =$  length( $T_1$ ) to  $i + 1$  do
    if  $|\lambda(j)| < |\lambda(j - 1)|$  then
      swap  $\lambda(j)$  with  $\lambda(j - 1)$ 
      swap  $s(j)$  with  $s(j - 1)$ 
    end
  end
end

```

\ \ obtain partitioned $S = \begin{pmatrix} S_1 & S_3 \\ S_2 & S_4 \end{pmatrix}$

$$G_{0,0} = [Z_{0,0} + Z_{0,1}(Z_{1,1} + Z_{1,2}S_2S_1^{-1})^{-1}Z_{1,0}]^{-1}$$

Algorithm 8: TMM for two semi-infinite crystals separated by another crystal slab

Initialization:

$$T_1 = \begin{pmatrix} \mathbf{0} & I \\ -Z_{1,2} & \mathbf{0} \end{pmatrix}, T_2 = \begin{pmatrix} I & \mathbf{0} \\ Z_{1,1} & Z_{2,1} \end{pmatrix},$$

$$\bar{T}_1 = \begin{pmatrix} \mathbf{0} & I \\ -\bar{Z}_{1,2} & \mathbf{0} \end{pmatrix}, \bar{T}_2 = \begin{pmatrix} I & \mathbf{0} \\ \bar{Z}_{1,1} & \bar{Z}_{2,1} \end{pmatrix}$$

Eigenanalysis $T_2S = T_1SA$

\ \ sort all the eigenvalues λ and the corresponding eigenvectors s in Λ and S

```

for  $i = 1$  to length( $T_1$ ) do
  for  $j =$  length( $T_1$ ) to  $i + 1$  do
    if  $|\lambda(j)| < |\lambda(j - 1)|$  then
      swap  $\lambda(j)$  with  $\lambda(j - 1)$ 
      swap  $s(j)$  with  $s(j - 1)$ 
    end
  end
end

```

\ \ obtain partitioned $S = \begin{pmatrix} S_1 & S_3 \\ S_2 & S_4 \end{pmatrix}$

Eigenanalysis $\bar{T}_2\bar{S} = \bar{T}_1\bar{S}\bar{A}$

\ \ sort all the eigenvalues $\bar{\lambda}$ and the corresponding eigenvectors \bar{s} in $\bar{\Lambda}$ and \bar{S}

```

for  $i = 1$  to length( $\bar{T}_1$ ) do
  for  $j =$  length( $\bar{T}_1$ ) to  $i + 1$  do
    if  $|\bar{\lambda}(j)| < |\bar{\lambda}(j - 1)|$  then
      swap  $\bar{\lambda}(j)$  with  $\bar{\lambda}(j - 1)$ 
      swap  $\bar{s}(j)$  with  $\bar{s}(j - 1)$ 
    end
  end
end

```

\ \ obtain partitioned $\bar{S} = \begin{pmatrix} \bar{S}_2 & \bar{S}_4 \\ \bar{S}_1 & \bar{S}_3 \end{pmatrix}$

$$G_{0,0} = [Z_{0,0} + Z_{0,1}(Z_{1,1} + Z_{1,2}S_2S_1^{-1})^{-1}Z_{1,0} + \bar{Z}_{0,1}(\bar{Z}_{1,1} + \bar{Z}_{1,2}\bar{S}_2\bar{S}_1^{-1})^{-1}\bar{Z}_{1,0}]^{-1}$$

The authors acknowledge the support from the National Natural Science Foundation of China Excellent Young Scientists Fund (HKU 12222417), the Hong Kong Research Grants Council Early Career Scheme (27300924), the Hong Kong Research Grant Council Strategic Topics (STG3/E-704/23-N), the startup fund of The University of Hong Kong, the Asian Young Scientist Fellowship and the Croucher Foundation. M. -Y. Xia acknowledges the support from the National Natural Science Foundation of China (62231001 and 62171005). L. Lu acknowledges the support from the Natural Science Foundation of China (12025409), the Beijing Natural Science Foundation (Z200008), the Chinese Academy of Sciences through the Project for Young Scientists in Basic Research (YSBR-021) and the International Partnership Program with the Croucher Foundation (112111KYSB20200024).

REFERENCES

- * yxsha@hku.hk
 † yiyg@hku.hk
- [1] L. Lu, J. D. Joannopoulos, and M. Soljačić, Topological photonics, *Nature photonics* **8**, 821 (2014).
 - [2] T. Ozawa, H. M. Price, A. Amo, N. Goldman, M. Hafezi, L. Lu, M. C. Rechtsman, D. Schuster, J. Simon, O. Zilberberg, *et al.*, Topological photonics, *Reviews of Modern Physics* **91**, 015006 (2019).
 - [3] S. Ma, B. Yang, and S. Zhang, Topological photonics in metamaterials, *Photonics Insights* **1**, R02 (2022).
 - [4] X. Zhang, M. Xiao, Y. Cheng, M.-H. Lu, and J. Christensen, Topological sound, *Communications Physics* **1**, 97 (2018).
 - [5] G. Ma, M. Xiao, and C. T. Chan, Topological phases in acoustic and mechanical systems, *Nature Reviews Physics* **1**, 281 (2019).
 - [6] H. Xue, Y. Yang, and B. Zhang, Topological acoustics, *Nature Reviews Materials* **7**, 974 (2022).
 - [7] Z.-D. Zhang, S.-Y. Yu, H. Ge, J.-Q. Wang, H.-F. Wang, K.-F. Liu, T. Wu, C. He, M.-H. Lu, and Y.-F. Chen, Topological surface acoustic waves, *Physical Review Applied* **16**, 044008 (2021).
 - [8] L. Yu, H. Xue, and B. Zhang, Topological slow light via coupling chiral edge modes with flatbands, *Applied Physics Letters* **118**, 071102 (2021).
 - [9] Y. Lumer and N. Engheta, Topological insulator antenna arrays, *ACS photonics* **7**, 2244 (2020).
 - [10] Z. Zhang, Y. Tian, Y. Wang, S. Gao, Y. Cheng, X. Liu, and J. Christensen, Directional acoustic antennas based on valley-hall topological insulators, *Advanced Materials* **30**, 1803229 (2018).
 - [11] T. Wu, Y. Li, X. Feng, S. Wu, Z. Gao, and L. Feng, Topological photonic lattice for uniform beam splitting, robust routing, and sensitive far-field steering, *Nano Letters* **23**, 3866 (2023).
 - [12] J.-Q. Wang, Z.-D. Zhang, S.-Y. Yu, H. Ge, K.-F. Liu, T. Wu, X.-C. Sun, L. Liu, H.-Y. Chen, C. He, *et al.*, Extended topological valley-locked surface acoustic waves, *Nature communications* **13**, 1324 (2022).
 - [13] M. A. Bandres, S. Wittek, G. Harari, M. Parto, J. Ren, M. Segev, D. N. Christodoulides, and M. Khajavikhan, Topological insulator laser: Experiments, *Science* **359**, eaar4005 (2018).
 - [14] Y. Zeng, U. Chattopadhyay, B. Zhu, B. Qiang, J. Li, Y. Jin, L. Li, A. G. Davies, E. H. Linfield, B. Zhang, *et al.*, Electrically pumped topological laser with valley edge modes, *Nature* **578**, 246 (2020).
 - [15] M. Farmanbar, T. Amlaki, and G. Brocks, Green’s function approach to edge states in transition metal dichalcogenides, *Physical Review B* **93**, 205444 (2016).
 - [16] S. Smidstrup, D. Stradi, J. Wellendorff, P. A. Khomyakov, U. G. Vej-Hansen, M.-E. Lee, T. Ghosh, E. Jónsson, H. Jónsson, and K. Stokbro, First-principles green’s-function method for surface calculations: A pseudopotential localized basis set approach, *Physical Review B* **96**, 195309 (2017).
 - [17] G. Metalidis and P. Bruno, Green’s function technique for studying electron flow in two-dimensional mesoscopic samples, *Physical Review B* **72**, 235304 (2005).
 - [18] J. Velez and W. Butler, On the equivalence of different techniques for evaluating the green function for a semi-infinite system using a localized basis, *Journal of Physics: Condensed Matter* **16**, R637 (2004).
 - [19] F. Guinea, C. Tejedor, F. Flores, and E. Louis, Effective two-dimensional hamiltonian at surfaces, *Physical Review B* **28**, 4397 (1983).
 - [20] M. L. Sancho, J. L. Sancho, and J. Rubio, Quick iterative scheme for the calculation of transfer matrices: application to mo (100), *Journal of Physics F: Metal Physics* **14**, 1205 (1984).
 - [21] M. L. Sancho, J. L. Sancho, J. L. Sancho, and J. Rubio, Highly convergent schemes for the calculation of bulk and surface green functions, *Journal of Physics F: Metal Physics* **15**, 851 (1985).
 - [22] D. Lee and J. Joannopoulos, Simple scheme for surface-band calculations. i, *Physical Review B* **23**, 4988 (1981).
 - [23] D. Lee and J. Joannopoulos, Simple scheme for surface-band calculations. ii. the green’s function, *Physical Review B* **23**, 4997 (1981).
 - [24] D. Lee and J. Joannopoulos, Renormalization scheme for the transfer-matrix method and the surfaces of wurtzite znO, *Physical Review B* **24**, 6899 (1981).
 - [25] D. H. Lee and J. D. Joannopoulos, A new theory of electronic surface states, *Journal of Vacuum Science and Technology* **19**, 355 (1981).
 - [26] Y.-C. Chang and J. Schulman, Complex band structures of crystalline solids: An eigenvalue method, *Physical Review B* **25**, 3975 (1982).
 - [27] M. B. Nardelli, Electronic transport in extended systems: Application to carbon nanotubes, *Physical Review B* **60**, 7828 (1999).
 - [28] I. Rungger and S. Sanvito, Algorithm for the construction of self-energies for electronic transport calculations based on singularity elimination and singular value decomposition, *Physical Review B* **78**, 035407 (2008).
 - [29] M. G. Reuter, T. Seideman, and M. A. Ratner, Probing the surface-to-bulk transition: A closed-form constant-scaling algorithm for computing subsurface green functions, *Physical Review B* **83**, 085412 (2011).
 - [30] C. H. Lewenkopf and E. R. Mucciolo, The recursive green’s function method for graphene, *Journal of Computational Electronics* **12**, 203 (2013).
 - [31] Y. Peng, Y. Bao, and F. von Oppen, Boundary green functions of topological insulators and superconductors, *Physical Review B* **95**, 235143 (2017).
 - [32] Q. Wu, S. Zhang, H.-F. Song, M. Troyer, and A. A. Soluyanov, Wanniertools: An open-source software package for novel topological materials, *Computer Physics Communications* **224**, 405 (2018).
 - [33] Y.-X. Sha, B.-Y. Liu, H.-Z. Gao, H.-B. Cheng, H.-L. Zhang, M.-Y. Xia, S. G. Johnson, and L. Lu, Surface density of states on

- semi-infinite topological photonic and acoustic crystals, *Physical Review B* **104**, 115131 (2021).
- [34] Z.-Y. Li and K.-M. Ho, Light propagation in semi-infinite photonic crystals and related waveguide structures, *Physical Review B* **68**, 155101 (2003).
- [35] M. Che and Z.-Y. Li, Analysis of surface modes in photonic crystals by a plane-wave transfer-matrix method, *JOSA A* **25**, 2177 (2008).
- [36] E. N. Economou, *Green's functions in quantum physics*, Vol. 7 (Springer Science & Business Media, 2006).
- [37] R. Carminati, A. Cazé, D. Cao, F. Peragut, V. Krachmalnicoff, R. Pierrat, and Y. De Wilde, Electromagnetic density of states in complex plasmonic systems, *Surface Science Reports* **70**, 1 (2015).
- [38] W. C. Chew, W. E. Sha, and Q. Dai, Green's dyadic, spectral function, local density of states, and fluctuation dissipation theorem, *Progress In Electromagnetics Research* **166**, 147 (2019).
- [39] J.-M. Jin, *The finite element method in electromagnetics* (John Wiley & Sons, 2015).
- [40] L. Novotny and B. Hecht, *Principles of nano-optics* (Cambridge university press, 2012).
- [41] T. Ma and G. Shvets, All-si valley-hall photonic topological insulator, *New Journal of Physics* **18**, 025012 (2016).
- [42] H. Yoshimi, T. Yamaguchi, Y. Ota, Y. Arakawa, and S. Iwamoto, Slow light waveguides in topological valley photonic crystals, *Optics Letters* **45**, 2648 (2020).
- [43] Y. Poo, R.-x. Wu, Z. Lin, Y. Yang, and C. T. Chan, Experimental realization of self-guiding unidirectional electromagnetic edge states, *Physical Review Letters* **106**, 093903 (2011).
- [44] C. He, X. Ni, H. Ge, X.-C. Sun, Y.-B. Chen, M.-H. Lu, X.-P. Liu, and Y.-F. Chen, Acoustic topological insulator and robust one-way sound transport, *Nature physics* **12**, 1124 (2016).
- [45] A. Pick, B. Zhen, O. D. Miller, C. W. Hsu, F. Hernandez, A. W. Rodriguez, M. Soljačić, and S. G. Johnson, General theory of spontaneous emission near exceptional points, *Optics express* **25**, 12325 (2017).
- [46] C. W. Hsu, B. Zhen, A. D. Stone, J. D. Joannopoulos, and M. Soljačić, Bound states in the continuum, *Nature Reviews Materials* **1**, 1 (2016).
- [47] C. Yue, Y. Xu, Z. Song, H. Weng, Y.-M. Lu, C. Fang, and X. Dai, Symmetry-enforced chiral hinge states and surface quantum anomalous hall effect in the magnetic axion insulator $\text{Bi}_2\text{-xSm}_x\text{Se}_3$, *Nature Physics* **15**, 577 (2019).